EARTHQUAKE SCENARIO GROUND MOTION MAPS FOR THE SAN FRANCISCO BAY REGION FOR A REPEAT OF THE M 7.9, 1906 EARTHQUAKE

Walter Silva[1], Ivan Wong[2], John Schneider[3]

ABSTRACT

For a repeat of the **M** 7.9 1906 San Francisco earthquake, ground shaking maps are produced for the ten Bay Area Counties. The maps include the effects of surficial soils and combine numerical region specific simulations with updated (2005) empirical attenuation relations appropriate for the western U.S. Based on comparisons with an earlier effort using a 1997 knowledge base, short period ground motions are expected to be dramatically reduced ($\geq$ 50%) at all distances while long period motions remain largely unchanged. The updated knowledge base, driven by several recent large earthquakes, is expected to have profound impacts on short period structures as well as liquefaction assessment.

Introduction

The US Geological Survey Working Group on California Earthquake Probabilities (WGCEP, 2003) recently completed a comprehensive review of the probabilities of occurrence of major earthquakes in the San Francisco Bay region (SFBR). Their report, "Earthquake Probabilities in the San Francisco Bay Region: 2002-2031", concludes that the probability of occurrence of a major earthquake in the region is about 70% over the next 30 years (WGCEP, 2003). The area of interest to this study is shown in Figure 1, which covers a 10-county region surrounding San Francisco with major population centers shown relative to active faults in the area. The study focuses on a key scenario event identified from the WGCEP (2003) report, a moment magnitude (**M**) 7.9 on the San Andreas fault, a repeat of the **M** 7.9 1906 earthquake. The San Andreas fault earthquake represents a rupture of the four northern segments of the fault, along a 473-km length from just north of Santa Cruz in the south, to Petrolia in the north. This scenario event is widely believed to be the most significant to consider for disaster planning and for the design of major structures in this area and has a mean return period of 378 yrs (WGCEP, 2003).

Ground Motion Modeling Approach

Based on the location and magnitude of the earthquake scenario, ground motions are first modeled for a uniform rock outcrop over a grid of about 600 points throughout the region. Rock motions are generated in terms of 5% damped acceleration response spectra at a suite of four periods from PGA (0 sec) to 3 sec (0, 0.2, 1.0 and 3.0 sec). Two different modeling approaches are used to generate the rock motions. In the first approach, a numerical simulation model is used to approximate the effects of the finite earthquake source rupture as well as regionally-specific parameters (Silva et al., 1990). Combined with the regionally-specific simulations, a suite of widely accepted western U.S. (WUS) empirical relations are used to generate corresponding rock

[1] Pacific Engineering and Analysis, 311 Pomona Ave., El Cerrito, CA 94530
[2] URS Corporation, 1333 Broadway, Ste. 800, Oakland, CA 94612
[3] Geoscience Australia, Cnr Jerrabomberra Avenue and Hindmarsh Dr., SYMONSTON ACT 2609, Camberra ACT 2601

outcrop motions. The empirical relations reflect both 1997 versions as well as recent preliminary updates resulting from the recent PEER Next Generation Attenuation (NGA) project.

Figure 1. Map of San Francisco Bay Area Counties, Key Cities, and Mapped Active Faults.

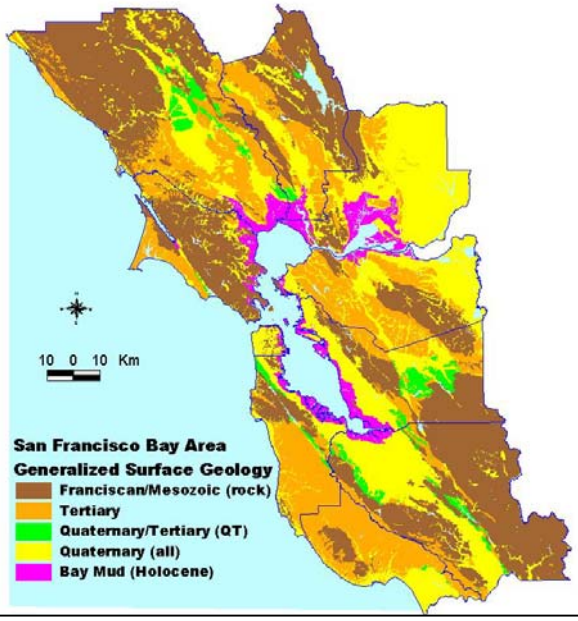

Figure 2. Map of Surface Geology for the San Francisco Bay Area.

Amplification factors are then applied to accommodate the effects of near-surface variability in geologic properties of soils, and for their depths to bedrock. A map of the soil classification based on geologic age is shown in Figure 2 (after Wentworth, 1997). The bedrock depths (Franciscan and Salinian) are based on Revision 1 of the Bay Area 3-D velocity model (Jachens, personal communication). These two databases, together with available seismic and geotechnical soils data provide for the development of a set of ground motion amplification factors for the SFBR for a wide range of input (rock) ground motion levels and spectral periods. The amplification factors are then applied to each set of rock motions based on the appropriate combination of surface geology, depth to bedrock, period of motion, and, expected rock peak ground acceleration input level. The resulting ground motions are combined to generate dense spatial grids of some 20,000 points of ground motions for each scenario. Empirical ground motions are combined with the stochastic simulations with weights of 0.4 and 0.6 respectively. The larger weight for the simulations is intended to reflect an emphasis on region-specific attributes such as static stress drop, Q(f) model, and crustal structure as well as the degree of validation for the simulation procedure. Final results are provided as a series of scenario hazard maps for expected median (50^{th} percentile) ground motions.

Scenario Specification

Rupture dimensions and the locations for individual fault segments are provided by WGCEP (1999) and presented in Table 1. For the purposes of modeling the ground motion, the locations and dimensions of the scenario are defined by the single plane rectangular plane that best satisfies the linear combination of segments. A single plane approximation is adequate, given the small deviations in azimuth of the fault in the Bay Area. The model values are summarized in Table 2. The scenario length is given simply by the sum of segment lengths, and the width is given by the

average value that preserves total fault area and seismic moment: average width = sum (L x W)/sum(L). For the San Andreas fault rupture, the average width over the four segments is 11.88 km, but the average width within the San Francisco Bay Area is ~ 13 km, a value that preserves rupture area and seismic moment within the area of interest for our ground motion calculations. The rupture plane is assumed to be vertical, and the mechanism is assumed to be right-lateral strike-slip.

The equivalent circular rupture Brune stress drop ($\Delta\sigma$) is 40 bars (Table 2) (46 bars using segment areas), considerably larger than the approximately 30 bars implied by the Wells and Coppersmith (1994) empirical magnitude/rupture area relation, more consistent with the Hanks and Bakun (2002) model of increasing stress drop with **M**. This increased static stress drop appears not to have a large impact on strong ground motions, as evidenced by a number of recent large earthquakes, captured in the updated NGA attenuation relations as well the finite fault simulations.

Table 1. Segmentation Parameters for the San Andreas Fault

Fault segment	Length (km)	Seismic Width (km)
SAF - North Coast North	135	11
SAF - North Coast South	191	11
SAF - Peninsula	85	13
SAF - Santa Cruz Mountains	62	15

Table 2. Characteristics of The San Andreas Earthquake Scenario.

Fault Rupture	Segments	Fault type	Length (km)	Avg Seismic Width (km)	Modeled Width (km)	M	$\Delta\sigma$ (Bars)
San Andreas	Santa Cruz Mountains, Peninsula, Southern North Coast, Northern North Coast	right-lateral strike-slip	473	12	13	7.9	40

Stochastic Fault Simulations

To accommodate finite-source effects, a methodology that combines the aspects of finite earthquake source modeling techniques (Hartzell, 1978) with the stochastic point source ground motion model (Boore, 1983) has been developed with motions estimated using random vibration theory (RVT) (Schneider et al., 1993; Silva et al., 1997). Finite source parameters include a constant slip velocity (to reduce dependence of motions on static stress drop) of 100 cm/sec and subevent stress-drop of 60 bars. Based validations of the approach (Silva et al, 1997), the subevent stress drop was reduced to 10 bars to accommodate the observed reduction in short-period motions for shallow-slip dominated earthquakes. In the earlier suite of maps, the subevent stress-drop was not reduced, resulting in short-period motions consistent with the 1997 (Abrahamson and Shedlock, 1997) empirical relations. Vertically propagating shear-waves combined with kappa (Anderson and Hough, 1984) are assumed for amplification while geometrical attenuation from each subfault to the site is modeled via the method of Ou and Herrmann (1990), along with a Q(f) term for crustal damping. The method is fundamentally broadband and a validation exercise using the Loma Prieta earthquake is discussed in Schneider et al. (1993). The model has recently been validated using about fifteen earthquakes and about 500 sites (Silva et al., 1997). An example of the validation exercise showing both variability and bias estimates, based on modeling recorded motions (5% damped spectra), for six (about 300 sites and distances to about 150 km) of the most relevant

earthquakes are shown in Figure 3. The broadband model is largely unbiased and captures site-to-site variations acceptably well, over a very wide frequency range.

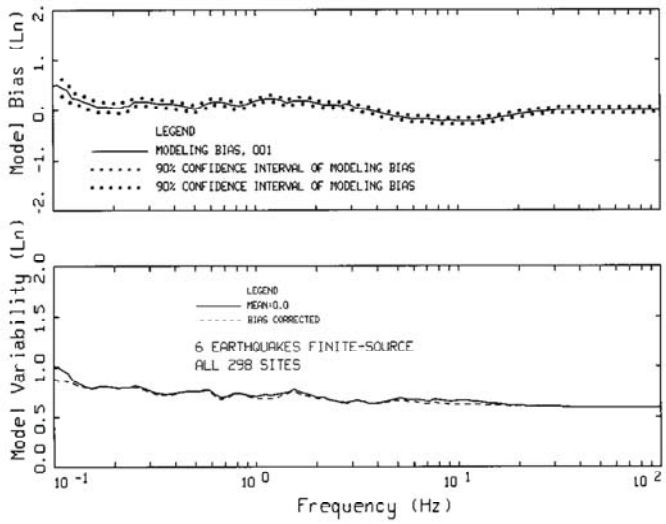

Figure 3. Finite Fault Validation Results for Six Largest, Best Recorded, and Relevant (of 15) Earthquakes: 1979 **M** 6.5 Imperial Valley, 1989 **M** 6.9 Loma Prieta, 1994 **M** 6.7 Northridge, 1992 **M** 7.2 Landers, 1995 **M** 6.9 Kobe, and 1999 **M** 7.4 Kocaeli.

Regionally-specific parameters for the SFBR (Table 3) have been determined from inversions of ground motion recordings from the 1989 Loma Prieta, 1979 Coyote Lake, and 1982 Morgan Hill earthquakes at about 90 sites over the fault distance range of about 12 to 90 km (Silva et al., 1997). The path damping, Q(f), and kappa value are randomized (Table 3) based on distributions from inversions (EPRI, 1993). These recordings have also been used to validate the EPRI (1993) nonlinear dynamic material properties used in developing the site amplification factors. As with the amplification factors, the shallow profile is for Franciscan rock outcropping (Table 5), merged into the Wald et al. (1991) crust. Generic rock G/Gmax and hysteretic damping curves (Silva et al., 1997) are used for materials with shear-wave velocities of 3,000 ft/sec. Finite source parameters including nucleation point and slip model have been randomized as well to simulate variations in rupture directivity and asperity location (Schneider, 2000).

Table 3. Source and Path Parameters Used in the Stochastic Simulation Model

Q_o	σ_{lnQo}	η	σ_η	κ (sec)	$\sigma_{ln\kappa}$
176	0.4	0.6	0	0.04	0.3

Empirical Attenuation Relations

As part of a recent PEER NGA project, five WUS empirical attenuation relations were updated (Next Generation Attenuation) using a common, greatly expanded strong motion and recording site condition database. Notable in the expanded database is the inclusion of several recent large earthquakes:1999 **M** 7.4 Kocaeli, Turkey;1999 **M** 7.6 Chi Chi, Taiwan; 1999 **M** 7.1, Duzce, Turkey; 1999 **M** 7.1 Hector Mine; 2002 **M** 7.8 Denali, Alaska. Recordings from these earthquakes confirmed earlier findings by Silva et al., (1997), in a simulation validation exercise using recordings from seventeen earthquakes at over 500 sties, that large earthquakes dominated by shallow slip (e.g. coseismic surface rupture) showed significantly lower short-period motions than corresponding deep slip dominated earthquakes. As a direct consequence, for large magnitude (**M** $\geq$ 7) crustal earthquakes, the updated NGA empirical relations show these trends in reduced short-

period motions. To illustrate the impact of the updated knowledge in expected motions, previously produced maps (Schneider et al., 2000) are compared to current estimates of motions. For the previous maps, the 1997 versions (Abrahamson and Shedlock, 1997) of four commonly used relations (Table 4) were implemented along with the same simulation methodology. In the current maps, preliminary NGA versions of three of the previously used four relations were available at the time the paper was prepared. Table 4 lists the previous and current relations along with assumptions made in implementing the models. A notable aspect of the NGA relations is the site description, now based on the average shear-wave velocity to a depth of 30m ($\overline{V}_S$(30m)), greatly reducing ambiguity in applications.

Table 4 Key Assumptions for Empirical Ground Motion Relations; 1997 and 2005

Relations	**Distance Measure**	**Depth of top of fault (km)**	**Parameters for 1997"Rock" relations, (V_s30) for 2005 relations**
Boore et al (1997)	To surface projection of rupture (R_{JB})	0	V_s30 = 511.10m/s(Geomatrix A/B category)
Abrahamson and Silva (1997, 2005)	To rupture surface (R_{rup})	0	"rock", V_s(30m) = 771 m/sec
Campbell(1997),Campbell & Bozorgnia(2005)	To top of rupture surface (R_{seismo})	3	"soft rock", V_s(30m) = 771 m/sec
Sadigh et al (1997), Chiou & Youngs (2005)	To rupture surface (R_{rup})	0	"rock", V_s(30m) = 771 m/sec

For the 1997 relations, the $\overline{V}_S$(30m) for typical soft rock in California is 511.10 m/s (Wills and Silva, 1998). This velocity is consistent with the Geomatrix category A/B used by Sadigh et al. (1997) and Abrahamson and Silva (1997) for rock motions and the "soft-rock" coefficients for Campbell (1997). The amplification factors were applied to these soft rock relations. While not strictly correct, since outcropping Franciscan reflects firm rock conditions ($\overline{V}_S$(30m) = 771 m/sec, Table 5), the potential error is not considered significant for this comparison. For the preliminary 2005 relations, their expected values are computed for the Franciscan $\overline{V}_S$(30m) value of 771 m/sec (Table 5).

Site Amplification

The SFBR site amplification factors were developed in a PEER sponsored project (Silva et al., 1999) and, for ease of application, based on simplified surface geology (Wills and Silva, 1998). Appropriate shear-wave velocity profiles were developed for each geologic type, based on measured profiles. The factors accommodate nonlinear rock/soil site response through an RVT based equivalent-linear approach (Silva et al., 1999) and are expressed as functions of expected Franciscan firm rock peak acceleration (up to 1.25g) as well as profile depth to 1 km/sec basement material.

The soil amplification factors are based on the separation of rock units into Franciscan and Tertiary units. Soil units consist of Quaternary-Tertiary, Quaternary and Older alluvium (generic Quaternary), and Bay Mud. Table 5 lists the geology types, $\overline{V}_S$(30m), the corresponding NEHRP site categories, and number of shear-wave velocity profiles in each category. Unfortunately, the median Bay Mud profile (Q_m), with its $\overline{V}_S$(30m) of about 188m/sec, is placed in NEHRP Category D, with firm soils (Table 5).

Three sets of G/Gmax and hysteretic damping curves are used: Franciscan and Tertiary rock are represented by curves developed for generic rocks (Silva et al., 1997). For cohesionless soils, which represent gravels, sands, and low plasticity-index clays, the EPRI (1993) G/Gmax and hysteretic damping curves are used. Quaternary/Tertiary rocks (QT_S) are also included in this grouping, consistent with their near-surface shear-wave velocity (800 ft/sec) and NEHRP site classification (C) (Table 4). For the Bay Mud (Q_m) categories, generic sections of artificial fill (15 ft), young Bay Mud (50 ft) and old Bay Clay (30 ft) over Quaternary Alluvium (Q_{al}) are assumed. These generic zones are based on an examination of several CALTRANS boreholes located near highway bridges (Cliff Roblee, personal communication) and are used only to assign G/Gmax and hysteretic damping curves. For the fill material and the alluvium, EPRI (1993) curves are used. For the young Bay Muds and Old Bay Clay, the Vucetic and Dobry (1991) cohesive soil curves for a PI of 40%, an average value for these cohesive soils, are used. All soils are constrained to be linear in response below 500 ft, based on modeling recorded motions (Silva et al., 1997).

To smooth over profile resonances and provide stable estimates of median and sigma values, profile parameters are randomized. Profile depth is randomized to generate mean category depth bins (Table 6), velocities and layer thicknesses are randomized based on a correlation model resulting from an analysis of variance on about 500 measured profiles (EPRI, 1993). G/Gmax and hysteretic damping curves are also randomized about based case models assuming a log-normal distribution (σ_{ln} = 0.35 at a shear-strain of 3 x 10^{-2}%) with $\pm$ 2σ bounds, all based on laboratory dynamic tests.

It is important to note that these amplification factors do not explicity incorporate basin (3D) effects. The San Andreas rupture considered here is a basin margin fault, which would result in much less excitation of surface waves in the basin relative to more distant events. While basin edge effects have been suggested to contribute strong near-source 2D effects, such as the heavily damaged zone in Kobe, Japan, other analyses have shown simple 1D effects based on local geology easily explain patterns of observed damage, motions, and observations of liquefaction (Silva et al., 1999; 2002). Additionally, source, path, and site modeling of 48 Bay area sites which recorded the Loma Prieta, Coyote Lake, and Morgan Hill earthquakes using a 1D soil model showed no bias associated with deep soil sites (Schneider et al., 1993; Silva et al., 1997). Hartzell et al. (1999) compare 1D and 3D source, path, and site modeling for sites in the Los Angeles basin that recorded the Northridge earthquake and show no difference in accuracy for response and Fourier amplitude spectra over the frequency range of 0.1 to 20 Hz. As a result, we conclude that neglecting potential basin effects will not result in a stable and serious underprediction of long period motions.

Table 5. Surface Geology Based Profiles, Site Classes, and Dynamic Material Properties.

Geology	Average Velocity over 30m (m/sec)	NEHRP Site Class	Number of Profiles	G/Gmax and Hysteretic Damping
Franciscan Bedrock (K_{jf})	771.44	B	30	Generic rock
Tertiary (TM_{zs})	506.13	C	18	Generic rock
Quaternary/Tertiary (QT_s)	466.12	C	9	EPRI
Quaternary Alluvium (Q_{al} + Q_{oa})	312.15	D	53	EPRI
Bay mud (Q_m)	187.87	D	60	Vucetic/Dobry,EPRI

Table 6. Depth Categories and Depth Ranges

Category	Geologic Units	Mean Depth (m)	Range (m)
1	Franciscan Bedrock (K_{jf})	N/A	N/A
2	Tertiary (TM_{zs})	N/A	N/A
3a	Quaternary/Tertiary (QT_s)	75	10 - 140
3b	Quaternary/Tertiary (QT_s)	150	100 - 200
4a	Quaternary Alluvium ($Q_{al} + Q_{oa}$)	75	10 -140
4b	Quaternary Alluvium ($Q_{al} + Q_{oa}$)	150	100-200
4c	Quaternary Alluvium ($Q_{al} + Q_{oa}$)	225	150 – 300
5a	Bay Mud (Q_m)	75	10 – 140
5b	Bay Mud (Q_m)	150	100 - 200

Development of Maps

The weighted mean [μln(Sa)] ground motion over all models is

$$\mu_{\ln(Sa)soil} = \sum_{i=1}^{n} W_i \left[\mu_{\ln(Sa_i)rock} + \mu_{Ln[Amp(Sa_i)]}\right], \quad (1)$$

and the variance from the weighted combination of different models is

$$Var[\ln(Sa)_{soil}] = \sum_{i=1}^{n} W_i \left[\sigma^2_{\ln(Sa_i)soil}\right] = \sum_{i=1}^{n} W_i \left[\sigma^2_{\ln(Sa_i)rock} + \sigma^2_{\ln[Amp(Sa)]_i}\right], \quad (2)$$

which does not include the additional variance contributed by the epistemic variability (different means) between models for rock. The total variance is

$$Var[\ln(Sa)_{soil}] = \sum_{i=1}^{n} W_i \left[\mu^2_{\ln(Sa_i)soil} + \sigma^2_{\ln(Sa_i)soil}\right] - \mu^2_{\ln(Sa)soil}. \quad (3)$$

To illustrate the differences between the updated expected median motions and previous values, Fig. 4 shows new maps compared to the 2000 versions (Schneider et al., 2000). The difference in short period motions is dramatic, with expected median peak acceleration values along the rupture reduced from about 1g to about 0.5g. For the East Bay and San Jose areas, the reduction is less, about 30% to 50%, likely due to soil nonlinearity. Similar trends are seen for 0.2 sec 5% spectral accelerations with the degree of reduction decreasing with increasing period. At 1 sec the updated motions along the rupture are in the 0.5g range compared to the 2000 map with a values closer to 0.8g. In the East Bay and San Jose areas, the expected 1 sec median motions have been reduced from about 0.5g to about 0.3g, close to a 60% reduction. At long period, 3 sec, the reduction is much less, with about 0.15g along the rupture for the updated maps compared to about 0.2g for the previous estimates. These differences in expected median motions at short-period are dramatic, and will likely have a significant impact on design, especially for liquefaction assessment. The differences are driven, both in the updated NGA empirical relations as well as the finite-fault simulations, by recent large world wide earthquakes and their relevance for applications to the WUS in general, and California in particular, is an issue which needs to be addressed.

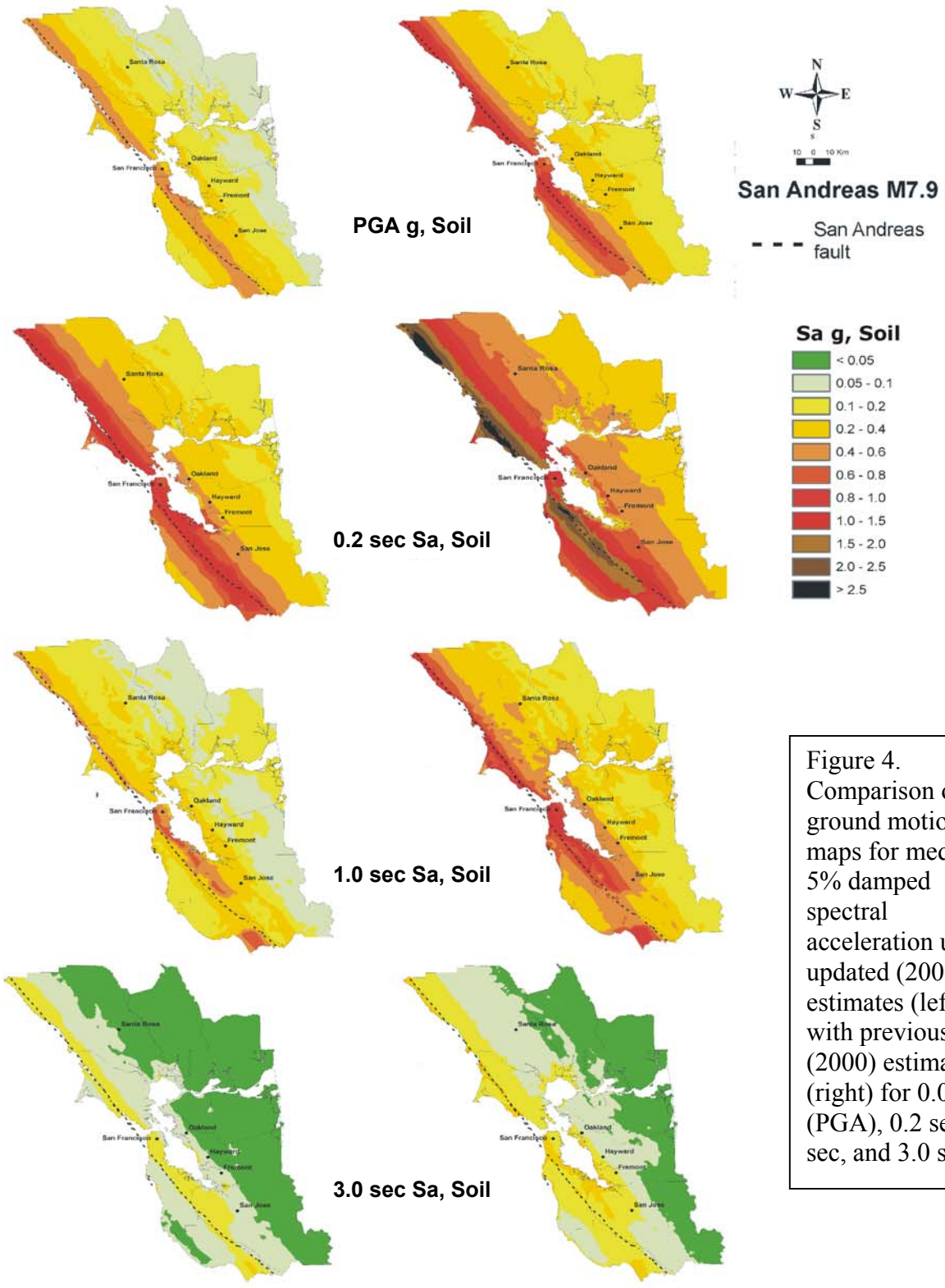

Figure 4. Comparison of ground motion maps for median 5% damped spectral acceleration using updated (2005) estimates (left) with previous (2000) estimates (right) for 0.01 sec (PGA), 0.2 sec, 1.0 sec, and 3.0 sec.

Conclusions

Comparisons of expected median motions between updated expectations, empirical (preliminary NGA) relations and finite-fault simulations, and previous expectations for a repeat of the 1906 **M** 7.9 San Andreas earthquake in the SFBR showed a general dramatic reduction (50% to 100%) in short period motions. The degree of reduction decreased with increasing period, showing a small reduction at a period of 3 sec. Both the updated empirical relations and finite-fault simulations, at large **M**, are driven by recent large worldwide earthquakes which showed dramatically reduced short-period motions compared to expected values based on current published empirical relations (Abrahamson and Shedlock, 1997). Relevance of these data to WUS and, in particular, California earthquake shaking hazard is an issue yet to be resolved.

Acknowledgements

The authors gratefully acknowledge PEER support for the surficial soil dependent amplification factors and especially the NGA project. We are grateful for the efforts of Doug Wright in producing the updated maps and to the Professional Development Programs of URS and Pacific Engineering and Analysis.

References

Abrahamson, N.A and K.M. Shedlock (1997). "Overview." *Seis. Research Lett.,* 68(1), 9-23.

Anderson, J. G. and S. E. Hough (1984). "A Model for the Shape of the Fourier Amplitude Spectrum of Acceleration at High Frequencies." *Bull. Seism. So. Am*., 74(5), 1969-1993.

Boore, D.M. (1986). "Short-period P- and S-wave Radiation from Large Earthquakes: Implications for Spectral Scaling Relations." *Bull. Seism. Soc. Am.,* 76(1) 43-64.

Boore, D.M. (1983). "Stochastic Simulation of High-Frequency Ground Motions Based On Seismological Models of the Radiated Spectra." *Bull. Seism. Soc. Am.*, 73, 1865-1894.

Borcherdt, R. D. and Glassmoyer, G. (1992). "On the characteristics of local geology and their influence on ground motions generated by the Loma Prieta Earthquake in the San Francisco Bay region, California." *Bull. Seism. Soc. Am.*, 82(2), 603-641.

Campbell, K W. (1997). "Empirical near-source attenuation relationships for horizontal and vertical components of peak ground acceleration, peak ground velocity, and pseudo absolute acceleration response spectra." *Bull. Seism. Soc. Am.*, 68(1), 154_179.

Electric Power Research Institute (1993). "Guidelines for determining design basis ground motions." Palo Alto, Calif: Electric Power Research Institute, vol. 1-5, EPRI TR-102293.

Hanks, T.C., and W.H. Bakun. (2002). "A bilinear source-scaling model for **M**-log *A* observations of Continental earthquakes." *Bull. Seismol. Soc. Am.,* 92(5), 1841-1846.

Hartzell, S., S. Harmsen, A. Frankel, and S. Larsen (1999). "Calculation of broadband time histories of ground motion: comparison of methods and validation using strong-ground motion from the 1994 Northridge earthquake." *Bull. Seism. Soc. Am.,* 89(6), 1484-1504.

Hartzell, S.H. (1978). "Earthquake aftershocks as Green's functions." *Geophys. Res. Let.,* 5, 1-4.

Ou, G.B., and Herrmann, R.B. (1990). "A statistical model for ground motion produced by earthquakes at local and regional distances." *Bull. Seism. Soc. Am.,* 80, 1397-1417.

Sadigh, C._Y. Chang, J.A. Egan, F. Makdisi, and R.R. Youngs (1997). "Attenuation relationships for shallow crustal earthquakes based on California strong motion data." *Seism. Soc. Am*., 68(1), 180_189.

Schneider, J. and W. J. Silva, and D. Wright (2000). "Earthquake scenario ground motion hazard maps for the San Francisco Bay region." *USGS Grant Award* #98-HQ-GR-1004, Final Report.

Schneider, J.F., W.J. Silva, and C.L. Stark (1993). Ground motion model for the 1989**M** 6.9 Loma Prieta ea rthquake including effects of source, path and site. *Earthquake Spectra,* 9(2), 251-287.

Silva, W.J, R. Darragh and N. Gregor (2002). "Incorporation of earthquake source, propagation path, and site uncertainties into assessment of liquefaction potential: Phase 1, validation" USGS Award #02-HQ-GR-0022.

Silva, W.J., S. Li, R. Darragh, and N. Gregor (1999). "Surface geology based strong motion amplification factors for the San Francisco Bay and Los Angeles areas" Final Report to Pacific Earthquake Engineering Research Center, University of California, Berkeley.

Silva, W.J., N. Abrahamson, G. Toro and C. Costantino. (1997). "Description and validation of the stochastic ground motion model." Report Submitted to Brookhaven National Laboratory, Associated Universities, Inc. Upton, New York 11973, Contract No. 770573

Vucetic, M.; Dobry, R. (1991). "Effects of Soil Plasticity on Cyclic Response," *Journal of Geotechnical Engineering, ASCE*, 117(1), 89-107.

Wald, D.J., D.V. Helmberger, and T.R. Heaton (1991). "Rupture model of the 1989 Loma Prieta Earthquake from the inversion of strong motion and broadband teleseismic data." *Bull. Seism. Soc. Amer*., 81(5), 1540-1572.

Wentworth, C.M. (1997). General distribution of geologic materials in the San Francisco Bay Region, California: A digital map database, US Geological Survey Open-File Report 97-744.

Wills, C.J, and W.J. Silva (1998). Shear-wave velocity characteristics of geologic units in California, *Earthquake Spectra*, 14:3, 533-556.